Nano Energy 89 (2021) 106330

Contents lists available at ScienceDirect

Nano Energy

journal homepage: www.elsevier.com/locate/nanoen

Triboelectric bending sensor based smart glove towards intuitive multi-dimensional human-machine interfaces

Yang Luo [a,1], Zihan Wang [a,1], Jiyu Wang [a], Xiao Xiao [b], Qian Li [c], Wenbo Ding [a,*], H.Y. Fu [a,*]

[a] Tsinghua Shenzhen International Graduate School and Tsinghua-Berkeley Shenzhen Institute, Tsinghua University, Shenzhen 518055, China
[b] Department of Bioengineering, University of California, Los Angeles, Los Angeles, CA 90095, United States
[c] School of Electronic and Computer Engineering, Peking University, Shenzhen 518055, China

ARTICLE INFO

Keywords:
Triboelectric nanogenerator
Angle sensor
Glove-based HMI
Machine learning recognition
Robotics

ABSTRACT

Recent advances in human-machine interface (HMI) lead to a renewed interest in creating intuitive and immersive interaction. Here, we designed a simple-structured and high-resolution bending angle triboelectric sensor named bending-angle triboelectric nanogenerator (BA-TENG) to construct a glove-based multi-dimensional HMI. With the assistance of a customized print circuit board (PCB), the glove-based HMI exhibits high sensitivity and low crosstalk in real-time multi-channel finger motion sensing. The signal-to-noise ratio (SNR) is improved by 19.36 dB. By systematically extracting and analyzing the multi-dimensional signal features of the BA-TENG, intuitive multi-dimensional HMIs were realized for smart-home, advanced robotic control, and a virtual keyboard with user recognition functionality. The classification accuracy of the virtual keyboard for seven users reached 93.1% by leveraging the advanced machine learning technique. The proposed BA-TENG-based smart glove reveals its potential as a solution for minimalist-design and intuitive multi-dimensional HMI, promising in diversified areas, including the Internet of things (IoT), assistive technology, and intelligent recognition systems.

1. Introduction

With the popularization of computers, machines, and robotics in recent decades, human-machine interfaces (HMIs), serving as bridges between human and machines, have demonstrated great significance and received tremendous attention. The classical HMIs, such as joysticks, keyboards, and touchpads, could meet the requirements in most scenarios but still have their limitations, especially when a more natural and intuitive manipulating manner is needed for virtual reality (VR) and augmented reality (AR). In this context, new types of HMIs that directly express human intentions are emerging as essential alternatives by leveraging other human features [1]. For instance, the electromyogram (EEG) [2], electromyography (EMG) [3], voice [4], and facial expression [5]. Among them, the HMI based on finger motions has attracted significant interest from the community due to its high precision and multiple degrees of freedom control [6–8]. Specifically, the finger motion, mainly from finger phalanxes, can be detected by glove-based HMI and projected into different machine commands, enabling immersive control in entertainment, healthcare systems, and manufacturing [9,10]. To this end, various sensors are customized to collect such information, for example, the inertial measurement unit (IMU) [11], resistive sensors [12,13], and capacitive sensors [14–16]. These sensors provide high accuracy in detecting finger motions [17,18], yet various challenges remain to be solved, such as temperature dependence, complicated fabrication, and low yields [11,19]. Besides, for low-weight and long-term connectivity, the power consumption of the HMI should also be optimized and minimized at the system level [19].

Triboelectric nanogenerator (TENG), as an emerging mechanical-to-electrical conversion technique, has been recognized as an appealing method to construct low-power or even self-powered sensors due to its nature of coupling contact electrification and electrostatic induction [20–23]. Moreover, thanks to the low cost, variety of material choices, and simple structure, TENG-based sensors have been widely applied to realize HMI functions in the form of keyboards and touchpads [24–31]. Furthermore, the unique working mechanism of TENG enables it to perceive subtle finger motions, making it an ideal candidate for the glove-based HMI [32–39]. On this basis, wearable HMI is fulfilled with the help of TENG, including robot control [8,25,36], the Internet of

* Corresponding authors.
E-mail addresses: ding.wenbo@sz.tsinghua.edu.cn (W. Ding), hyfu@sz.tsinghua.edu.cn (H.Y. Fu).
[1] These authors contributed equally.

https://doi.org/10.1016/j.nanoen.2021.106330
Received 6 May 2021; Received in revised form 5 July 2021; Accepted 7 July 2021
Available online 9 July 2021

things (IoT) [38,40], and hand gesture recognition [41–47]. However, two significant challenges exist in the current work. On the one hand, since most of the research utilizes only the limited feature (i.e., the TENG 's output voltage) to characterize finger motions, it is sometimes farfetched to characterize finger's continuous movements and diversified gestures with a single sensor[8,19,44,48–50]. In this context, extreme complications in the structure and electrode design are usually introduced in the related work [51–53], requiring extra power consumption in signal processing and hindering the users from manipulating HMI intuitively and effectively. On the other hand, crosstalk in multi-channel sensing needs to be better solved. Since TENG essentially has high resistance and a small current, coupling effects may occur between adjacent channels through the capacitance of the analog-to-digital converter (ADC) [8]. To realize real-time multi--channel HMI, these constraints need to be overcome.

Herein, we report a wearable glove-based system for real-time intuitive multi-dimensional HMI. With the assistance of this system, analog triboelectrification signals generated by finger motions can be converted to the digital domain, as shown in Fig. 1a. Our system shows good sensitivity, low crosstalk, and intuitive manipulating experience. The real-time signal-to-noise ratio (SNR) was improved by 19.36 dB using the customized glove-based system. To illustrate the capabilities of the glove-based HMI, multi-dimensional signal features are extracted from the bending angle triboelectric nanogenerators (BA-TENG) to achieve light control (the bending angle and speed), advanced robotic hand control (the bending angle, speed, and hold time), and a virtual 9-digit keyboard with user identification (multi-dimensional features), as shown in 1a. A total of 350 keystroke dynamics for a password that contains multi-dimensional signal features [54] were generated by the virtual keyboard. The glove-based HMI demonstrates a high recognition rate of 93.1% against 7 different users by leveraging a machine learning algorithm. This work exhibits promising applications of the BA-TENG-based smart glove towards multi-dimensional HMIs, including smart IoT, assistive technology, and intelligent recognition systems.

2. Results and discussion

2.1. Glove-based system

The glove-based system consists of BA-TENG and a wireless customized PCB, as shown in Fig. 1b and Fig. S1. Owing to the simple structure design and the use of two soft and flexible materials, polydimethylsiloxane (PDMS) and silicone rubber, the BA-TENG can conform to the skin of human fingers when detecting finger motions. BA-TENG converts finger motions into triboelectric signals. The wireless customized PCB worn on the wrist realizes signal conditioning, processing, and wireless transmission through available integrated circuit components, as shown in Fig. 1b. The numbered boxes indicate the locations of the integrated circuit components that correspond to the functions in the block diagram of the glove-based system in Fig. 1c. Fig. 1c provides an overview of the process flow of signal conditioning. The analog signal acquired in each BA-TENG is independently amplified by a multi-channel trans-impedance amplifier. Then, the amplified signals experience signal processing, ADC conditioning, wireless transmission and finally received by a customized terminal display. The 5-channel trans-impedance amplifier independently amplifies the triboelectric output from different BA-TENGs and avoids the crosstalk from adjacent channels. A commodity microcontroller integrated with an ATmega 328P microprocessor and nRF24L01+ wireless communication module realizes computational and serial communication functions. Our glove-based multi-dimensional HMI system adopts an arch structure BA-TENG, with minimal system design and sensor layout. Besides, the system achieves sensitive motion detection, crosstalk avoidance, and multi-dimensional human-machine interaction. Four sets of signal features can be extracted from BA-TENG and projected to multi-function robotic control. As summarized in Table S1, compared with other works that only use the limited signal features (signal amplitude and peak numbers), our system can control the robotic hand in grabbing level, speed, and holding time, with intuitive logics between finger motions and the commands. Additionally, the virtual keyboard based on the system offers a new version in human-machine interaction, which has a relatively high identification accuracy for seven users, as presented in Table S2.

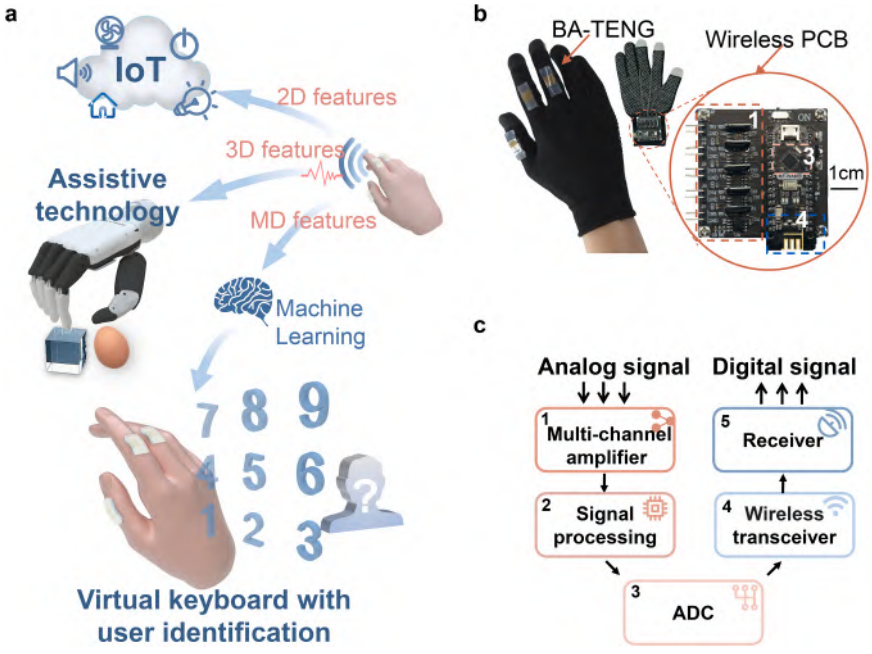

Fig. 1. (a) Schematic illustrations of the BA-TENG-based intuitive HMI for the intelligent IoT, assistive technology, and a virtual keyboard with user identification. (b) Photograph of the glove-based HMI components, including BA-TENG array and a wireless printed circuit board (PCB). The dashed boxes indicate the location of the integrated components. (c) Circuit diagram of signal flow in real-time HMI, from the acquired analog signals to the digital signals.

2.2. Structural design and working mechanism

A simple-structured, easy to fabricate, self-powered, and high-resolution BA-TENG is developed to input front-end information into the circuit system. As illustrated in Fig. 2a, the BA-TENG comprises two pieces of commercially viable materials, PDMS and silicone rubber, serving as negative and positive materials due to their different restraint capability of electrons. The detailed fabricating process of the BA-TENG is presented in Fig. S2 and Experimental section. The softness and flexibility of the two materials enable the BA-TENG to fit the finger surface closely. As a result, BA-TENG offers precise motion detection and better manipulating experience than the sensors that tend to separate from the finger in the bending-release cycle [34,35,55]. The embedded Cu mesh serves as an electrode (Fig. S3), which offers good flexibility under the deformation of the BA-TENG [56]. Bending deformation of the BA-TENG brings about a change in the contact area between PDMS and silicone rubber in a bending-release cycle. Since these two materials have different restraint capabilities of electrons, a triboelectric potential builds up at the interfacial region [18,22,56] (the silicone rubber becomes positively charged while the PDMS becomes negatively charged, as schematically shown in Fig. 2a). A detailed testing condition and working mechanism of the BA-TENG are presented in Fig. S4. To visualize the stress and potential distribution in a bending-release cycle, COMSOL Multiphysics was used to show the deformation of the BA-TENG at the bending angle of 80° and 0°, respectively, corresponding to different stress distributions, as shown in Fig. 2b and Fig. S5. In the characterization, the bending angle of the BA-TENG indicates its force conditions. The simulation details are presented in Note S1.

2.3. Mechanical and electrical properties characterization

To investigate the viability of the BA-TENG in detecting finger motions, its mechanical and electrical properties is quantitatively characterized using an actuating motor to offer cyclic force. Fig. 2c compares the experimental data on the BA-TENG's sensitivity measurement in a bending angle range from 40° to 100° at a frequency of 2 Hz, covering that of the human finger in a normal bending range. The short-circuit current (I_{sc}) of the BA-TENG sees a nearly linear increase from 40° to 100°, corresponding to 22.1–138.4 pA, respectively. As shown in Fig. 2d, the corresponding open-circuit voltage (V_{oc}) at 40°, 50°, 60°, 70°, 80°, 90°, and 100° is 0.33 V, 0.74 V, 1.21 V, 1.62 V, 1.95 V, 2.27 V, and 2.52 V, respectively. The insert shows the enlarged view of the BA-

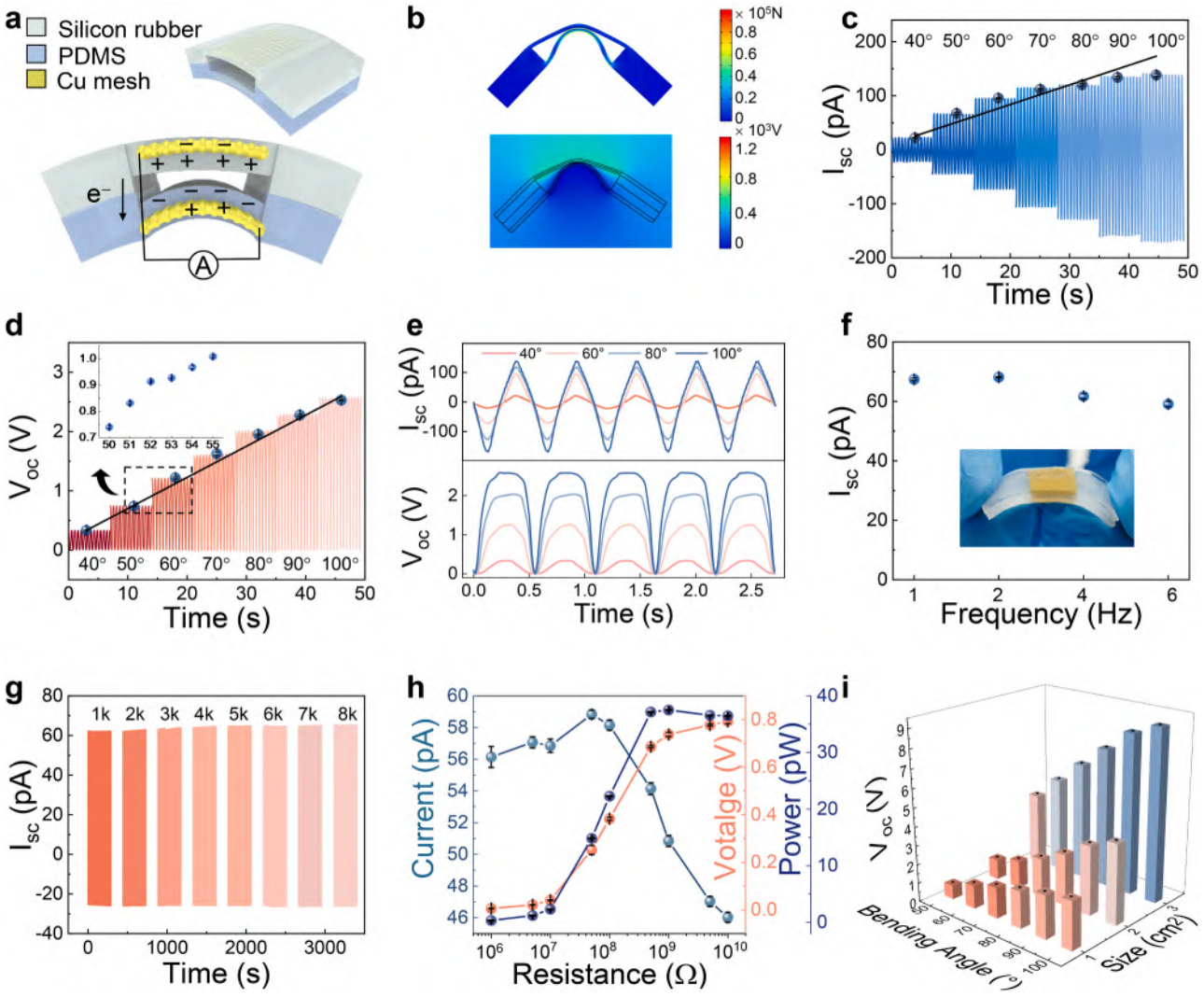

Fig. 2. (a) Schematic illustration of the working mechanism of the BA-TENG. (b) Stress and potential distribution of the BA-TENG at the bending angle of 80°. (c) Short-circuit current (I_{sc}) against bending angles. (d) Open-circuit voltage (V_{oc}) against bending angles. Insert, V_{oc} of each bending angle from 50° to 55°. (e) The profiles of I_{sc} and V_{oc}. (f) Frequency dependence of the output current at the bending angle of 50°. Insert shows the bending state of the BA-TENG. (g) Mechanical durability test for 8000 continuous bending cycles. (h) Dependence of the current, voltage, and power output on the external load resistance. (i) The output of the BA-TENG with different bending angles and sizes.

TENG's sensitivity ranging from 55° to 60°, indicating good angular resolution of the BA-TENG. The sensitivity is defined as $S = \Delta V / \Delta\theta$, where ΔV is the relative potential change and θ is the bending angle. A high bending angle resolution (0.04 V/°) is obtained in the wide strain range (40° ~ 100°). Detailed current and voltage profiles at various bending angles of 40°, 60°, 80°, and 100° are presented in Fig. 2e, indicating a stable and uniform output signal generated by the proposed simple-structured BA-TENG. Besides, the current dependence on the bending frequency at a bending angle of 50° is shown in Fig. 2f. The output voltage is 67.4 pA, 68.1 pA, 61.7 pA, and 59.1 pA at 1 Hz, 2 Hz, 4 Hz, and 6 Hz, respectively. Additionally, Fig. 2g presents the summary statistics for the mechanical durability of the BA-TENG. The output current remains relatively stable during 8000 continuous bending-release cycles at 50°. The result indicates good mechanical durability of the BA-TENG, which is beneficial in the long-term application. Furthermore, the output power of the BA-TENG was investigated with a wide range of external load resistances, as illustrated in Fig. 2h. The voltage amplitude increases with the load resistance, while the current follows a reverse trend. The instantaneous peak power maximizes at a load resistance of 1 GΩ, corresponding to a peak power of 37.5 pW. We also studied the output of the BA-TENG dependent on the device area. As shown in Fig. 2i, statistical tests reveal that the bending angle sensitivity could be obtained in various device sizes. The output voltage is proportional to the device size of BA-TENG.

2.4. Real-time triboelectric signal acquisition

The multi-channel real-time signal acquisition is usually performed using a single ADC and applies sequential scanning. However, with a low output current and high impedance, sequential scanning of multi-channel TENG input via a single ADC can lead to crosstalk and high noise in the signal. The trans-impedance amplifier (TIA) has recently been adopted in nanosensors to address these issues [57–59]. Fig. 3a illustrates the electronic design of the single-channel TIA ($R_1 = R_2 = R_3 = 10$ kΩ. $R_4 = 10$ GΩ. $R_5 = 500$k. $C_1 = C_2 = C_4 = 10$ μF. $C_3 = 1$ pF.), which converts the current input to the voltage output,

$$V_{out} = \frac{V_{cc}}{2} \pm I_{in} \times R_4.$$

As shown in Fig S6, the customized PCB can effectively avoid crosstalk, and the SNR is improved by 19.36 dB in real-time multi-channel finger motion sensing. To eliminate the effect of background noise and extract the signal features, the triboelectric signal in the receiving end is filtered, as presented in Fig. 3b. The motions of the human finger contain a wealth of information and can be developed for intuitive multi-dimensional HMI. However, current work focuses solely on the signal amplitude or peak number, as shown in Table S1, and defines it to various human-machine interaction commands. As a result, the functionality of HMI is limited while aggravating the system complexity and the uncomfortableness of users [51]. Herein, we extract four groups of the signal features of the BA-TENG, valley amplitude (V), hold time (H), valley width (W), and time interval (T), and develop

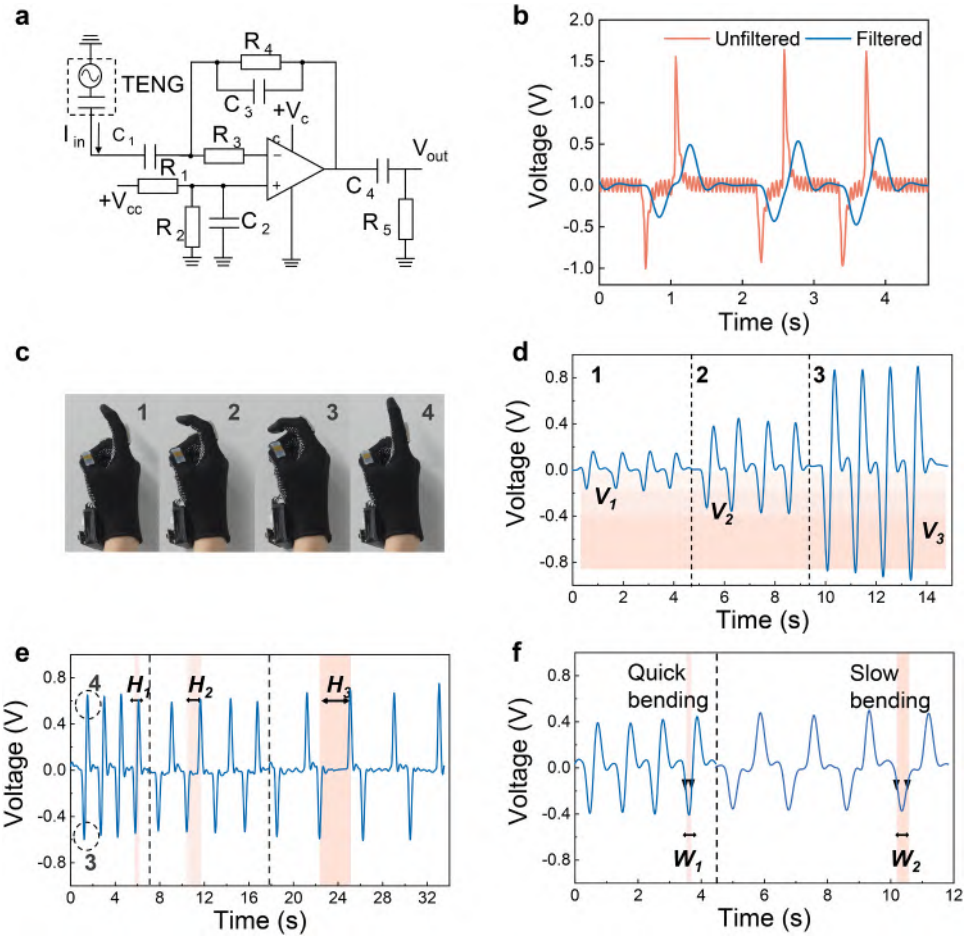

Fig. 3. Real-time triboelectric signal acquisition. (a) Electronic circuit of the single-channel trans-impedance amplifier. (b) Filtered and unfiltered output signals. (c) Photographs of three bending states of the index finger (1, 2, 3) and its release state (4). (d) The corresponding signal in (c). (e), (f) The signal with a different hold time (H) and valley width (W).

intuitive multi-dimensional HMI. Fig. 3c shows the bending motion of the index finger at different bending angles and its release status. The corresponding experimental data preprocessed by the customized PCB is presented in Fig. 3d. Note that the voltage data is transformed as a relative value for better understanding. Each motion is continuously repeated four times, demonstrating the reliability of output signals. It is attributed to the excellent bending angle resolution of the BA-TENG, as discussed in Fig. 2, enabling the signal amplitudes to express the bending levels of the finger.

Besides, the valley and the peak of the triboelectric signal correspond to the finger bending and releasing, respectively, as shown in Fig. 3e. Accordingly, the hold time (*H*), defined as the interval time between the signal valley and the signal peak in one bending-release cycle of fingers, can be extracted as another signal feature. Three sets of signal output with different *H* are compared in Fig. 3e. Additionally, the valley width of the triboelectric signal is affected by the bending speed of the finger. Here, the width is defined as the time when the voltage reaches and falls below 40% of the corresponding valley value, as shown in Fig. 3f. It can be seen that the quick bending of the finger causes a narrow valley width, while slow bending responds to a wide one. Hence, the continuous finger motion can be described by the valley width (*W*).

2.5. Demonstration of the intelligent IoT and robotic hand control

As a primary verification for the glove-based HMI for intelligent IoT and assistive technology, the detected triboelectric outputs were used to project the finger motions into light-brightness control and robotic hand control using multi-dimensional signal features. The circuit connection for the wireless light and robotic hand control is depicted in Fig. 1c. The receiver is connected to a microcontroller (MCU) for the light and robotic hand control. To intuitively demonstrate the signal profile and features of the triboelectric output, LabVIEW was used to visualize the signal processing on a computer. The experimental data on the bending angle resolution of the glove-based HMI is shown in Fig. 4a, where eight bending statuses of the finger can be explicitly distinguished. It is due to the BA-TENG unit's outstanding resolution to the bending angle. Note that each curve is relatively shifted by 0.5 V in the vertical axis for display purposes. The signal valley corresponds to the finger bending, as mentioned in the signal acquisition part. Therefore, light can be dimed at different levels corresponding to different finger bending angles, as shown in Fig. 4b and Video S1. Figs. 4b-1, 2, and 3 corresponds to the marked signal profiles in Fig. 4a. The glove offers more states than the state "on" and state "off" in light control, accommodating diversified smart home scenarios. Additionally, utilizing the signal's valley width, the bending speed of fingers could intuitively control the speed of the light liming, as shown in Fig. 4c and Video S1.

Supplementary material related to this article can be found online at doi:10.1016/j.nanoen.2021.106330.

Besides the amplitude and signal width, hold time is another indispensable signal feature of finger motions, depending on the bending time of fingers. Combing these three signal features, advanced robotic hand control can be achieved. Five BA-TENG were attached to the glove to detect each finger's motion. As defined in Fig. 3, the signal valley and peak of the triboelectric outputs are defined as commands of grab and release, respectively. Hold time (*H*) determines the grabbing time of the robotic hand; signal valley (*V*) controls the grabbing levels of the robotic hand, and the signal width (*W*) corresponds to the bending speed of the robotic hand. Fig. 4d shows the real-time voltage profiles of the finger motions. Note that the slight difference in signal magnitudes is ascribed to the different bending states of five fingers. To demonstrate the control of the robotic hand with different patterns, we pre-set the robotic hand with three hold time, three different gabbing levels, and two different grabbing speeds, which can be triggered by the output signal of the glove-based HMI. As shown in Video S2, for the control of the grabbing

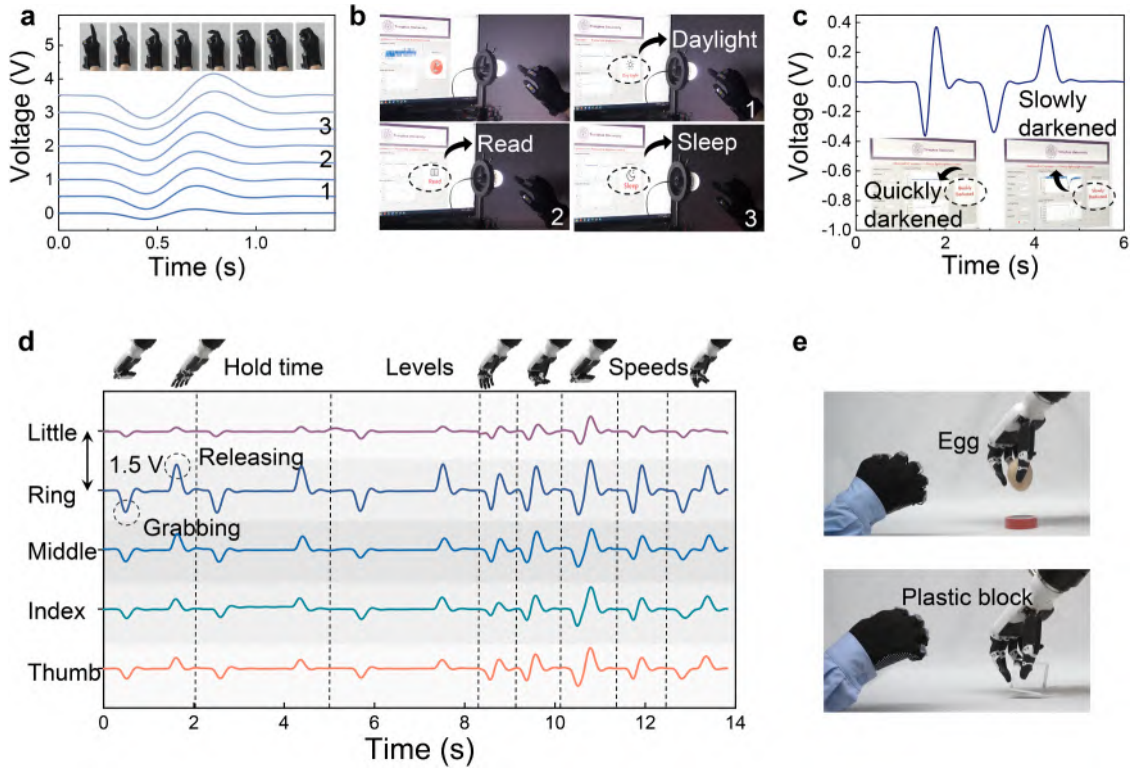

Fig. 4. Light-brightness control and advanced robotic control. (a) The real-time signal output from the index finger at eight bending angles. (b) Screenshots of the video showing the various light-brightness control through different finger bending angles. (c) Real-time signal output to control the speed of light dimming. (d) Real-time signal output to control a robotic hand with three different hold time (*H*), three different valley amplitudes (*V*), and two valley width (*W*). (e) Screenshots of the demonstration showing the advanced robotic hand control for different-object grab.

speed, at a slow bending speed of the finger where the valley width (*W*) of the signal is larger than the threshold, the robotic hand grabbed at a slow speed. Conversely, when the human finger bends quickly, generating a narrow valley width signal, the robotic hand recognized it and grabbed at fast accordingly. It works the same for grabbing with different levels and hold time. As a result, by analyzing the proposed three signal features from the BA-TENG, an advanced robotic hand control can be achieved from grabbing time, grabbing degree, and grabbing speed. The multi-dimensional and intuitive manipulating process reveals the BA-TENG's potential in assistive technology. As shown in Fig. 4e and Video S2, the robotic hand is controlled by the BA-TENG based glove to grab a plastic block and an egg at different grabbing speeds, preventing damages to the egg.

Supplementary material related to this article can be found online at doi:10.1016/j.nanoen.2021.106330.

2.6. Application of the machine-learning-assisted virtual keyboard with user identification

Glove-based HMI's recent advances have led to a renewed interest in a more intelligent and personalized system. Hence, the multi-dimensional detection of finger motions incorporated with advanced data analysis techniques is the key to the research of HMIs [35]. Machine learning has been widely used in the area of TENG-based HMI for data analysis, such as gait analysis [19,60], object recognition [37], sign-language recognition [46], and smart floor monitoring [61]. Herein, a customized SVM-based software platform was developed and integrated with the glove-based HMI to construct a user identification system (Fig. 5a). Three BA-TENGs serve to convert the finger bending into digital signals. Channel 1–3 corresponds to the thumb, index, and middle finger, respectively. Each channel corresponds to 3 digits according to different magnitudes of the signal valley. After investigating the voltage ranges generated by 7 users using glove-based HMI, we set the triggering voltage thresholds for the three numbers as − 0.15 V, − 0.225 V, and − 0.30 V, respectively; each number corresponds to a voltage range of 0.075 V (Fig. 5b). Therefore, a virtual keyboard can be realized by bending fingers at three different angles, thereby removing the constraints of a physical keyboard and widening its application.

Besides, for a number series generated by the virtual keyboard, the multi-dimensional keystroke features can be obtained using specific signal process techniques (Note S2, Supporting information), including signal magnitudes, signal width, and the time interval between two numbers. Since the keystroke dynamics is a biometric behavior, its ballistic nature and non-invasive monitoring characteristics make it a

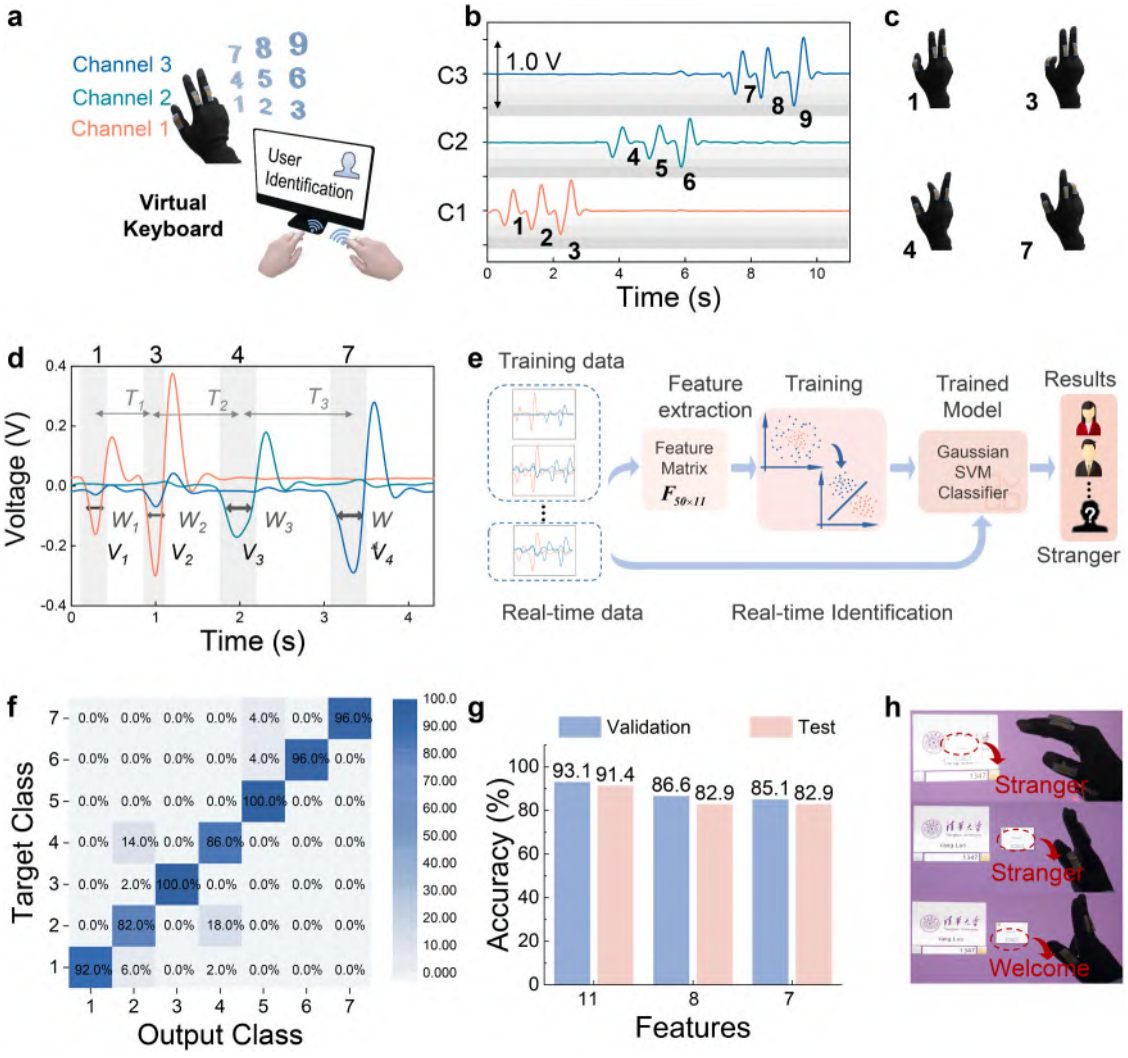

Fig. 5. (a) A virtual keyboard with user identification based on the smart glove (b) Real-time signal output of 9 numbers through 3 channels (C1-C3). (c) Finger motions to generate the password '1–3–4–7'. (d) Real-time password signals with 11 extracted features. (e) Process flow of the training and real-time identification. ((f) The Confusion maps of 7 participants using 11 signal features. (g) Classification accuracy using 11, 8, and 7 features, respectively. (h) Screenshots of the video demonstrating real-time user identification.

candidate for improving the recognition systems [54]. Here, for an exemplifying number sequence consisting of 4 digits "1–3–4–7″ (Fig. 5c), a total of 11 features can be extracted accordingly, the valley voltages of each number V_1, V_2, V_3, V_4, the valley widths of each number W_1, W_2, W_3, W_4, and the time intervals between each number T_1, T_2, T_3. V_i, W_i, (i = 1, 2, 3, 4) is defined in Fig. 3. T_i, (i = 1, 2, 3) is defined as the time between two adjacent signal valleys, as shown in Fig. 5d. A total of 350 sets of data were obtained from 7 users (50 for each), showing their typical typing behaviors using the virtual keyboard (Fig. S7). During the training process, the feature vectors of different users are used to build user profile modes via supervised learning with a support vector machine (SVM). The multi-class SVM classifier is generated by building multiple binary-class SVM classifiers, distinguishing one class of the acquired three-channel signal pattern and the rest (Note S3, Supporting information). In the real-time identification process, the trained multi-class SVM classifier is adopted to identify the users based on the feature pattern of the input data (Fig. 5e). The dataset is randomly divided for training (90%) and validation (10%). Fig. 5f shows the confusion matrix obtained from the 10-fold cross-validation classification with an overall validation accuracy of 93.1%. The output class represents the predicted results of the trained model. Additionally, the testing accuracy obtained from another 70 data (10 for each) is 91.4%. The good accuracy is attributed to the multi-dimensional signal features obtained from the smart glove. As shown in Fig. 5g, the dataset with eight-dimension features (V_1, V_2, V_3, V_4, W_1, W_2, W_3, W_4) has a lower validation and testing accuracy of 86.6% and 82.9%; the dataset with seven-dimension features (V_1, V_2, V_3, V_4, T_1, T_2, T_3) has a validation and testing accuracy of 85.1% and 82.9%, respectively. Fig. 5h provides an overview of the virtual keyboard with identification using the BA-TENG-based glove. The imposters knowing the correct password still cannot log into the computer systems unless the typing dynamics match the one registered in the system, as demonstrated in Video S3.

Supplementary material related to this article can be found online at doi:10.1016/j.nanoen.2021.106330.

3. Conclusions

Intuitive and immersive manipulating experience in human-machine interactions is the ultimate aim of glove-based HMIs. This requires not only the straightforward logic between human finger gestures and the projecting commands but also a minimalist design of the interface for a better manipulating experience to users. In this work, we proposed an alternative solution by designing a simple-structured and high bending angle resolution TENG and extracting multi-dimensional signal features from its triboelectric outputs. Consequently, diversified human-machine interactions, ranging from light-brightness control and advanced robotic hand control, have been successfully realized. Moreover, by leveraging the machine learning technique, a virtual keyboard with user identification is achieved by extracting keystroke dynamics patterns from multi-dimensional signal features. Benefit from the minimalist design, the proposed glove-based multi-dimensional HMIs can be readily produced on a large scale with low cost and easy fabrication. This work exhibits the applications of the proposed HMIs for the intelligent IoT, assistive technology, intelligent recognition systems, and more application areas with intuitive and immersive manipulating experiences.

4. Experimental section

4.1. BA-TENG fabrication

The simple-structured BA-TENG consists of two flexible and low-cost materials, PDMS and silicone rubber. A shape mold was used for fabricating both PDMS and silicone rubber films, as shown in Fig. S2. The PDMS was prepared by thoroughly mixing the base monomer and curing agent at a volume ratio of 10: 1 (Dow Corning Sylgard 184). The silicone rubber film was prepared by mixing its two components at a volume ratio of 1:1 (Ecoflex supersoft silicone 00-50, Smooth-On, Inc.). The gas bubbles in the two mixture were removed through 10-minute degasification at room temperature. Then the two mixture was injected in their molds, respectively. After partially cured at 80° for 20 min. Two Cu mesh electrodes were embedded in the PDMS and silicone rubber, respectively. Then the two films were cured entirely for 2 h. The TENG unit size is presented in Fig. S2d, where both PDMS and silicone rubber layers are 3 cm × 1 cm × 0.06 (± 0.02) cm, and the Cu mesh is 1 × 1 cm. The SEM images of the PDMS, silicone rubber, and Cu mesh are shown in Fig. S3.

4.2. Characterization and measurement

The morphology and microstructure of the Cu mesh, silicone rubber, and PDMS were characterized by Scanning electron microscopy (SEM, Hitachi SU8010). A programmable electrometer (Keithley 6514) was adopted to evaluate the electrical output of the BA-TENG. A linear motor system is used to provide cyclic stimuli in the measurement. The graphical user interface with real-time control and analysis was realized through LabVIEW® 2019 with MATLAB® module. Inspire-Robots, Beijing provided the controlled robotic hand (RH56DF3-XR/L). COMSOL Multiphysics software was employed for the simulation of the potential distribution. All the experiments were conducted at atmospheric pressure (1.01 × 105 Pa) and room temperature unless otherwise stated.

CRediT authorship contribution statement

H. Y. Fu. and W. Ding guided the whole project. Y. Luo. wrote the original draft. All authors discussed the results and commented on the manuscripts.

Declaration of Competing Interest

The authors declare that they have no known competing financial interests or personal relationships that could have appeared to influence the work reported in this paper.

Acknowledgment

The authors would appreciate S. Zhang (Tsinghua Shenzhen International Graduate School) for his help to this work. This work was supported by Shenzhen Science and Technology Innovation Commission (Project JCYJ20180507183815699, GJHZ20180411185015272), Tsinghua-Foshan Innovation Special Fund (TFISF) 2020THFS0109 the grant from the Institute for Guo Qiang, Tsinghua University 2020GQG1004, Guangdong Basic and Applied Basic Research Foundation 2020A1515110887, and the National Natural Science Foundation of China (Grant No. 52007019).

Appendix A. Supporting information

Supplementary data associated with this article can be found in the online version at doi:10.1016/j.nanoen.2021.106330.

References

[1] M. Zhu, T. He, C. Lee, Technologies toward next generation human machine interfaces: from machine learning enhanced tactile sensing to neuromorphic sensory systems, Appl. Phys. Rev. 7 (2020), 031305.
[2] Z. Xiang, J. Liu, C. Lee, A flexible three-dimensional electrode mesh: an enabling technology for wireless brain–computer interface prostheses, Microsyst. Nanoeng. 2 (2016) 1–8.
[3] S.J. Bensmaia, L.E. Miller, Restoring sensorimotor function through intracortical interfaces: progress and looming challenges, Nat. Rev. Neurosci. 15 (2014) 313–325.
[4] J. Shotton, T. Sharp, A. Kipman, A. Fitzgibbon, M. Finocchio, A. Blake, M. Cook, R. Moore, Real-time human pose recognition in parts from single depth images, Commun. ACM 56 (2013) 116–124.

[5] L.-Q. Tao, H. Tian, Y. Liu, Z.-Y. Ju, Y. Pang, Y.-Q. Chen, D.-Y. Wang, X.-G. Tian, J.-C. Yan, N.-Q.J.Nc Deng, An intelligent artificial throat with sound-sensing ability based on laser induced graphene, Nat. Commun. 8 (2017) 1–8.

[6] Y.-T. Tsai, W.-Y. Jhu, C.-C. Chen, C.-H. Kao, C.-Y. Chen, Unity game engine: interactive software design using digital glove for virtual reality baseball pitch training, Microsyst. Technol. 27 (2019) 1401–1417.

[7] F. Cini, V. Ortenzi, P. Corke, M. Controzzi, On the choice of grasp type and location when handing over an object, Sci. Robot. 4 (2019) eaau9757.

[8] M. Zhu, Z. Sun, A. Zhang, Q. Shi, T. He, H. Liu, C. Lee, Haptic-feedback smart glove as a creative human-machine interface (HMI) for virtual/augmented reality applications, Sci. Adv. 6 (2020) 8693.

[9] J.C. Yeo, C.T. Lim, Nanoengineering, emerging flexible and wearable physical sensing platforms for healthcare and biomedical applications, Microsyst. Nanoeng. 2 (2016) 1–19.

[10] M. Xie, K. Hisano, M. Zhu, T. Toyoshi, M. Pan, S. Okada, O. Tsutsumi, S. Kawamura, C. Bowen, Flexible multifunctional sensors for wearable and robotic applications, Adv. Mater. Technol. 4 (2019), 1800626.

[11] C. Metzger, E. Fleisch, J. Meyer, M. Dansachmüller, I. Graz, M. Kaltenbrunner, C. Keplinger, R. Schwödiauer, S. Bauer, Flexible-foam-based capacitive sensor arrays for object detection at low cost, Appl. Phys. Lett. 92 (2008), 013506.

[12] J. Eom, R. Jaisutti, H. Lee, W. Lee, J.-S. Heo, J.-Y. Lee, S.K. Park, Y.-H. Kim, Highly sensitive textile strain sensors and wireless user-interface devices using all-polymeric conducting fibers, Appl. Mater. Interfaces 9 (2017) 10190–10197.

[13] Y.-J. Liu, W.-T. Cao, M.-G. Ma, P. Wan, Ultrasensitive wearable soft strain sensors of conductive, self-healing, and elastic hydrogels with synergistic “soft and hard” hybrid networks, Appl. Mater. Interfaces 9 (2017) 25559–25570.

[14] M. Amjadi, A. Pichitpajongkit, S. Lee, S. Ryu, I. Park, Highly stretchable and sensitive strain sensor based on silver nanowire–elastomer nanocomposite, ACS Nano 8 (2014) 5154–5163.

[15] K. Suzuki, K. Yataka, Y. Okumiya, S. Sakakibara, K. Sako, H. Mimura, Y. Inoue, Rapid-response, widely stretchable sensor of aligned MWCNT/elastomer composites for human motion detection, ACS Sens. 1 (2016) 817–825.

[16] J. Kim, M. Lee, H.J. Shim, R. Ghaffari, H.R. Cho, D. Son, Y.H. Jung, M. Soh, C. Choi, S. Jung, Stretchable silicon nanoribbon electronics for skin prosthesis, Nat. Commun. 5 (2014) 1–11.

[17] S. Pyo, J. Choi, J. Kim, Flexible, transparent, sensitive, and crosstalk-free capacitive tactile sensor array based on graphene electrodes and air dielectric, Adv. Electron. Mater. 4 (2018), 1700427.

[18] H.-K. Kim, S. Lee, K.-S. Yun, Physical, capacitive tactile sensor array for touch screen application, Nat. Commun. 165 (2011) 2–7.

[19] Z. Zhang, T. He, M. Zhu, Z. Sun, Q. Shi, J. Zhu, B. Dong, M.R. Yuce, C. Lee, Deep learning-enabled triboelectric smart socks for IoT-based gait analysis and VR applications, npj Flex. Electron. 4 (2020).

[20] Z.L. Wang, A.C. Wang, On the origin of contact-electrification, Mater. Today 30 (2019) 34–51.

[21] C. Wu, A.C. Wang, W. Ding, H. Guo, Z.L. Wang, Triboelectric nanogenerator: a foundation of the energy for the new era, Adv. Energy Mater. 9 (2019), 1802906.

[22] F.-R. Fan, Z.-Q. Tian, Z. Lin Wang, Flexible triboelectric generator, Nano Energy 1 (2012) 328–334.

[23] A. Ahmed, I. Hassan, A.S. Helal, V. Sencadas, A. Radhi, C.K. Jeong, M.F. El-Kady, Triboelectric nanogenerator versus piezoelectric generator at low frequency (<4 Hz): a quantitative comparison, iScience 23 (2020), 101286.

[24] Q. Shi, Z. Zhang, T. Chen, C. Lee, Minimalist and multi-functional human machine interface (HMI) using a flexible wearable triboelectric patch, Nano Energy 62 (2019) 355–366.

[25] T. Chen, Q. Shi, M. Zhu, T. He, L. Sun, L. Yang, C. Lee, Triboelectric self-powered wearable flexible patch as 3D motion control interface for robotic manipulator, ACS Nano 12 (2018) 11561–11571.

[26] C. Qiu, F. Wu, C. Lee, M.R. Yuce, Self-powered control interface based on Gray code with hybrid triboelectric and photovoltaics energy harvesting for IoT smart home and access control applications, Nano Energy 70 (2020), 104456.

[27] Z.W. Yang, Y. Pang, L. Zhang, C. Lu, J. Chen, T. Zhou, C. Zhang, Z.L. Wang, Tribotronic transistor array as an active tactile sensing system, ACS Nano 10 (2016) 10912–10920.

[28] F. Xue, L. Chen, L. Wang, Y. Pang, J. Chen, C. Zhang, Z.L. Wang, MoS2 tribotronic transistor for smart tactile switch, Adv. Funct. Mater. 26 (26) (2016) 2104–2109.

[29] J. Zhao, H. Guo, Y.K. Pang, F. Xi, Z.W. Yang, G. Liu, T. Guo, G. Dong, C. Zhang, Z. L. Wang, Flexible organic tribotronic transistor for pressure and magnetic sensing, ACS Nano 11 (2017) 11566–11573.

[30] F. Xi, Y. Pang, W. Li, T. Bu, J. Zhao, G. Liu, T. Guo, W. Liu, C. Zhang, Tribotronic bipolar junction transistor for mechanical frequency monitoring and use as touch switch, Microsyst. Nanoeng. 4 (2018) 25.

[31] S. Hao, J. Jiao, Y. Chen, Z.L. Wang, X. Cao, Natural wood-based triboelectric nanogenerator as self-powered sensing for smart homes and floors, Nano Energy 75 (2020), 104957.

[32] Y. Cheng, D. Wu, S. Hao, Y. Jie, X. Cao, N. Wang, Z.L. Wang, Highly stretchable triboelectric tactile sensor for electronic skin, Nano Energy 64 (2019), 103907.

[33] T. Bu, T. Xiao, Z. Yang, G. Liu, X. Fu, J. Nie, T. Guo, Y. Pang, J. Zhao, F. Xi, Stretchable triboelectric–photonic smart skin for tactile and gesture sensing, Adv. Mater. 30 (30) (2018), 1800066.

[34] L. Dhakar, P. Pitchappa, F.E.H. Tay, C. Lee, An intelligent skin based self-powered finger motion sensor integrated with triboelectric nanogenerator, Nano Energy 19 (2016) 532–540.

[35] F. Wen, Z. Sun, T. He, Q. Shi, M. Zhu, Z. Zhang, L. Li, T. Zhang, C. Lee, Machine learning glove using self-powered conductive superhydrophobic triboelectric textile for gesture recognition in VR/AR applications, Adv. Sci. 7 (2020), 2000261.

[36] Y. Lee, S.H. Cha, Y.W. Kim, D. Choi, J.Y. Sun, Transparent and attachable ionic communicators based on self-cleanable triboelectric nanogenerators, Nat. Commun. 9 (2018) 1804.

[37] T. Jin, Z. Sun, L. Li, Q. Zhang, M. Zhu, Z. Zhang, G. Yuan, T. Chen, Y. Tian, X. Hou, C. Lee, Triboelectric nanogenerator sensors for soft robotics aiming at digital twin applications, Nat. Commun. 11 (2020) 5381.

[38] T. He, Z. Sun, Q. Shi, M. Zhu, D.V. Anaya, M. Xu, T. Chen, M.R. Yuce, A.V.-Y. Thean, C. Lee, Self-powered glove-based intuitive interface for diversified control applications in real/cyber space, Nano Energy 58 (2019) 641–651.

[39] S.S. Ham, G.-J. Lee, D.Y. Hyeon, Y.-g Kim, Y.-w Lim, M.-K. Lee, J.-J. Park, G.-T. Hwang, S. Yi, C.K. Jeong, K.-I. Park, Kinetic motion sensors based on flexible and lead-free hybrid piezoelectric composite energy harvesters with nanowires-embedded electrodes for detecting articular movements, Compos. Part B Eng. 212 (2021), 108705.

[40] J. Li, C. Wu, I. Dharmasena, X. Ni, Z. Wang, H. Shen, S.-L. Huang, W. Ding, Triboelectric nanogenerators enabled internet of things: a survey, Intell. Conv. Netw. 1 (2020) 115–141.

[41] M. Ha, S. Lim, S. Cho, Y. Lee, S. Na, C. Baig, H. Ko, Skin-inspired hierarchical polymer architectures with gradient stiffness for spacer-free, ultrathin, and highly sensitive triboelectric sensors, ACS Nano 12 (2018) 3964–3974.

[42] H. Zhang, W. Han, K. Xu, Y. Zhang, Y. Lu, Z. Nie, Y. Du, J. Zhu, W. Huang, Metallic sandwiched-aerogel hybrids enabling flexible and stretchable intelligent sensor, Nano Lett. 20 (2020) 3449–3458.

[43] X. Chen, Y. Song, H. Chen, J. Zhang, H. Zhang, An ultrathin stretchable triboelectric nanogenerator with coplanar electrode for energy harvesting and gesture sensing, J. Mater. Chem. A 5 (2017) 12361–12368.

[44] Q. He, Y. Wu, Z. Feng, W. Fan, Z. Lin, C. Sun, Z. Zhou, K. Meng, W. Wu, J. Yang, An all-textile triboelectric sensor for wearable teleoperated human–machine interaction, J. Mater. Chem. A 7 (2019) 26804–26811.

[45] L. Xie, X. Chen, Z. Wen, Y. Yang, J. Shi, C. Chen, M. Peng, Y. Liu, X. Sun, Spiral steel wire based fiber-shaped stretchable and tailorable triboelectric nanogenerator for wearable power source and active gesture sensor, Nanomicro Lett. 11 (2019) 39.

[46] Z. Zhou, K. Chen, X. Li, S. Zhang, Y. Wu, Y. Zhou, K. Meng, C. Sun, Q. He, W. Fan, E. Fan, Z. Lin, X. Tan, W. Deng, J. Yang, J. Chen, Sign-to-speech translation using machine-learning-assisted stretchable sensor arrays, Nat. Electron. 3 (2020) 571–578.

[47] S. Park, J. Park, Y.-g Kim, S. Bae, T.-W. Kim, K.-I. Park, B.H. Hong, C.K. Jeong, S.-K. Lee, Laser-directed synthesis of strain-induced crumpled MoS2 structure for enhanced triboelectrification toward haptic sensors, Nano Energy 78 (2020), 105266.

[48] Y.-C. Lai, J. Deng, S.L. Zhang, S. Niu, H. Guo, Z.L. Wang, Single-thread-based wearable and highly stretchable triboelectric nanogenerators and their applications in cloth-based self-powered human-interactive and biomedical sensing, Adv. Funct. Mater. 27 (2017), 1604462.

[49] X. Pu, H. Guo, Q. Tang, J. Chen, L. Feng, G. Liu, X. Wang, Y. Xi, C. Hu, Z.L. Wang, Rotation sensing and gesture control of a robot joint via triboelectric quantization sensor, Nano Energy 54 (2018) 453–460.

[50] K. Qin, C. Chen, X. Pu, Q. Tang, W. He, Y. Liu, Q. Zeng, G. Liu, H. Guo, C. Hu, Magnetic array assisted triboelectric nanogenerator sensor for real-time gesture interaction, Nano-Micro Lett. 13 (2021) 1–9.

[51] S. Sundaram, P. Kellnhofer, Y. Li, J.-Y. Zhu, A. Torralba, W. Matusik, Learning the signatures of the human grasp using a scalable tactile glove, Nature 569 (2019) 698–702.

[52] M. Cheng, X. Huang, C. Ma, Y.J. Yang, A flexible capacitive tactile sensing array with floating electrodes, J. Micromech. Microeng. 19 (2009), 115001.

[53] X. Wang, H. Zhang, L. Dong, X. Han, W. Du, J. Zhai, C. Pan, Z.L. Wang, Self-powered high-resolution and pressure-sensitive triboelectric sensor matrix for real-time tactile mapping, Adv. Mater. 28 (2016) 2896–2903.

[54] C. Wu, W. Ding, R. Liu, J. Wang, A.C. Wang, J. Wang, S. Li, Y. Zi, Z.L. Wang, Keystroke dynamics enabled authentication and identification using triboelectric nanogenerator array, Mater. Today 21 (2018) 216–222.

[55] J. Liao, Y. Zou, D. Jiang, Z. Liu, X. Qu, Z. Li, R. Liu, Y. Fan, B. Shi, Z. Li, L. Zheng, Nestable arched triboelectric nanogenerator for large deflection biomechanical sensing and energy harvesting, Nano Energy 69 (2020), 104417.

[56] Y. Luo, T. Zhao, Y. Dai, Q. Li, H.J.S. Fu, A.A. Physical, Flexible nanosensors for non-invasive creatinine detection based on triboelectric nanogenerator and enzymatic reaction, Sens. Actuators A Phys. 320 (2021), 112585.

[57] M. Crescentini, M. Bennati, M. Carminati, M. Tartagni, Noise limits of CMOS current interfaces for biosensors: a review, IEEE Trans. Biomed. Circuits Syst. 8 (2014) 278–292.

[58] D. Kim, B. Goldstein, W. Tang, F.J. Sigworth, E. Culurciello, Line-scanning particle image velocimetry: an optical approach for quantifying a wide range of blood flow speeds in live animals, PLoS One 7 (2012) 38590.

[59] J.-H. Noh, Frequency-response analysis frequency-response analysis and design rules for capacitive feedback transimpedance amplifier, IEEE Trans. Instrum. Meas. 69 (2020) 9408–9416.

[60] Y. Han, F. Yi, C. Jiang, K. Dai, Y. Xu, X. Wang, Z.J.N.E. You, Self-powered gait pattern-based identity recognition by a soft and stretchable triboelectric band, Nano Energy 56 (2019) 516–523.

[61] Q. Shi, Z. Zhang, T. He, Z. Sun, B. Wang, Y. Feng, X. Shan, B. Salam, C. Lee, Deep learning enabled smart mats as a scalable floor monitoring system, Nat. Commun. 11 (2020) 4609.

Yang Luo is now studying for a master's degree in Shenzhen International Graduate School, Tsinghua-Berkeley Shenzhen Institute (TBSI), Tsinghua University. He received a bachelor's degree from Northeastern University in 2019. His research interests are self-powered systems, including human-machine interactions and optical communication.

Zihan Wang received the dual BEng. degrees (1st class Hons.) from School of Telecommunications Engineering, Xidian University and Edinburgh Centre for Robotics, Heriot-Watt University, respectively in 2019. He is currently pursuing his MS degree in Data Science and Information Technology at Smart Sensing and Robotics (SSR) group, Tsinghua University. His research interests include self-powered sensors and robotics.

Jiyu Wang received his B.S. and Ph.D degrees from Department of Electrical Engineering, Chongqing University, Chongqing, China, in 2013 and 2019, respectively. He is currently a Post-Doctoral Fellow in Tsinghua-Berkeley Shenzhen Institute, Tsinghua University. His main research interests focus on the advanced electrical energy materials, triboelectric nanogenerator, semiconductors and their applications in self-powered sensor networks.

Xiao Xiao is a PhD student in the Department of Bioengineering at the University of California, Los Angeles under the supervision of Professor Jun Chen. Xiao obtained his Bachelor's degree in Materials Science and Engineering from Beihang University in 2020. His research focuses on wearable electronics and smart textiles for energy, sensing and therapeutic applications.

Qian Li received the B.S. degree from Zhejiang University, Hangzhou, China, in 2003, the M.Sc. degree from the Royal Institute of Technology (KTH), Stockholm, Sweden, in 2005, and the Ph.D. degree from the Hong Kong Polytechnic University, Hong Kong, in 2009. She is now an associate professor in School of Electronic and Computer Engineering (ECE) in Peking University. Her research interests include nonlinear optics, ultrafast optics, and integrated optics. Dr. Li is member of the Institute of Electrical and Electronics Engineers (IEEE) and a senior member of the Optical Society of America (OSA).

Wenbo Ding received the BS and PhD degrees (Hons.) from Tsinghua University in 2011 and 2016, respectively. He worked as a postdoctoral research fellow at Georgia Tech under the supervision of Prof. Z. L. Wang from 2016 to 2019. He is now a tenure-track assistant professor and PhD supervisor at Tsinghua-Berkeley Shenzhen Institute, Tsinghua Shenzhen International Graduate School, Tsinghua University, where he leads the Smart Sensing and Robotics (SSR) group. His research interests include self-powered sensors, energy harvesting, and wearable devices for health and soft robotics with the help of signal processing, machine learning, and mobile computing.

H. Y. Fu is currently an associate professor in Tsinghua-Berkeley Shenzhen Institute (TBSI), Tsinghua University. He received the B.S. degree in electronic and information engineering from Zhejiang University and the M.Sc. degree in electrical engineering with a specialty in photonics from Royal Institute of Technology, Stockholm, Sweden, and the Ph.D. degree from the Department of EE from Hong Kong Polytechnic University. His research interests include integrated photonics and its related applications, fiber optical communications, fiber optic sensing technologies. He is a senior member of the Institute of Electrical and Electronics Engineers (IEEE) and a life member of the Optical Society of America (OSA).